Hybrid Lidar-Radar Ocean Experiment

Linda J. Mullen, Peter R. Herczfeld, *Fellow, IEEE*, and Vincent M. Contarino

***Abstract*— This paper concerns a novel hybrid lidar-radar system for underwater surveillance. Simulations and laboratory measurements incorporating the hybrid detection scheme revealed a 17-dB suppression of the water backscatter signal (clutter) and corresponding target contrast enhancement. These results led to the design, implementation and testing of a lidar-radar system for ocean experimentation. Details of this system, in addition to the goals and results of the ocean experiment, are presented.**

I. Introduction

BLUE-GREEN LIDAR (light detection and ranging) is used for underwater surveillance. A pulse of optical radiation is transmitted from an airborne platform, and target information is extracted from the detected echo. Lidar has the potential for replacing acoustic techniques for underwater remote sensing. However, attenuation, dispersion, backscatter clutter and lack of coherent signal processing currently limit the performance of lidar in the detection of underwater objects.

In response to these shortcomings, a detection scheme has been developed by combining the sophisticated detection and signal processing techniques of microwave radar and the underwater transmission capability of lidar. In the hybrid configuration, the radar signal is impressed on the optical pulse by modulating the carrier at microwave frequencies. The reflected optical signal, together with the superimposed microwave envelope, is detected by a high-speed photodetector. The radar subcarrier is then recovered by a microwave receiver and processed independently from the lidar return. In this technique, both the optical carrier (lidar) and the microwave envelope (radar) are examined simultaneously from a single measurement.

A theoretical study was conducted to ascertain the ability of the hybrid scheme to improve the detection sensitivity of lidar [1]. In this analysis, the frequency response of the lidar return, $H_{dL}(f)$, was derived:

$$H_{dL}(f) = H_i(f) + H_t(f) = \left(\frac{\eta F A_r}{R^2}\right)\left\{\rho \frac{1 - e^{-2\alpha v t_d} e^{j4\pi f t_d}}{\alpha v - j2\pi f} \rho_t e^{-2\alpha v t_t} e^{j4\pi f t_t}\right\}$$

where η is the efficiency of the transmit and receive optics, F is a loss factor to account for an insufficient receiver field of view, A_R is the active area of the optical detector, and R is the platform altitude. The first term in brackets represents the backscatter frequency response, $H_i(f)$, while the second expression is the frequency response for an underwater target reflection, $H_t(f)$. Each term includes an exponential coefficient, α, which accounts for the attenuation of the optical signal due to absorption and scattering in the water. The backscatter and target reflectivities are represented by ρ and ρ_t, respectively. In addition, the search time, $t_d = L/v$ (where v is the speed of light in water), relates to the depth of the water column searched, L, while t_t is the time corresponding to the underwater target depth.

The amplitude frequency response, $|H_{dL}(f)|$, of a typical lidar return signal is shown in Fig. 1. The backscatter clutter portion, $|H_i(f)|$, decays for frequencies above the cut-off frequency, $f_c = \alpha v/2\pi$, which is estimated to be in the range of 2–10 MHz. The backscatter magnitude and cut-off frequency vary with the water clarity. However, the amplitude of the target reflection, $|H_t(f)|$, remains relatively independent of frequency if the target is small and interference effects are minimal. Superimposed on the background frequency response is the frequency spectrum of the transmitted modulated lidar pulse. The spectrum of the detected return signal consists of the product of the pulse frequency response with the background and target frequency spectra. The lidar receiver responds to the low frequency portion of the frequency response (<100 MHz), while the radar receiver recovers the spectrum component which is centered at the microwave modulation frequency (3 GHz). The main difference between the two signals is the relative magnitude of the target return to the backscatter clutter, which defines the target contrast. For the case represented in Fig. 1, the integrated backscatter dominates the signal in the lidar frequency range, and the target echo is buried in the clutter (i.e., $|H_i(f)| > |H_t(f)|$). Conversely, at the radar frequency, the decrease in backscatter clutter produces an improved target contrast. Thus, since the clutter is suppressed while the target remains unaffected, implementation of the hybrid detection scheme generates an enhanced target contrast relative to conventional lidar.

A laboratory setup incorporating an optical fiber based ocean mass simulator [2] was design and fabricated. With this setup, the capabilities of the hybrid system to reduce backscatter clutter and to enhance target contrast were evaluated. The microwave receiver included a bandpass filter centered at the 3-GHz modulation frequency, a microwave amplifier, and a microwave detector. The lidar receiver consisted of a low frequency (100 MHz) amplifier. The results confirmed the predictions that the backscatter clutter is suppressed by 17-dB relative to the lidar return and that the target contrast is improved by use of the hybrid detection scheme [1].

Manuscript received April 2, 1996. This work was supported in part by NAWC Contract N62269-93-C-0501 and by the NSF through the GEE Fellowship for Women and Minorities.

L. J. Mullen and P. R. Herczfeld are with the Center for Microwave-Lightwave Engineering, Drexel University, Philadelphia, PA 19104 USA.

V. M. Contarino is with the Naval Air Warfare Center, Aircraft Division, Patuxent River, MD 20607 USA.

Publisher Item Identifier S 0018-9480(96)08561-4.

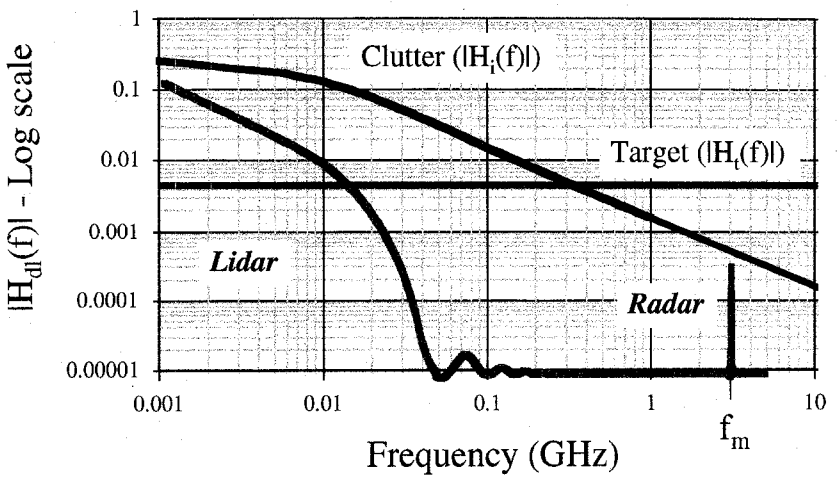

Fig. 1. Pictorial representation of the amplitude frequency response, $|H_{dl}(f)|$ of a lidar return signal, with a component for the backscatter, $|H_i(f)|$, and underwater target, $|H_t(f)|$. Also pictured is the modulated 10 nsec pulse frequency response. The detected return signal is the product of these two spectra and contains a low frequency (<100 MHz) component and one which is centered at the modulation frequency.

These analytical studies and laboratory experiments established the potential of the new approach for improving underwater target surveillance. In an actual ocean setting, three types of variables affect the measurements. The first kind concerns the properties of water: its clarity, depth, and sea state, all of which vary randomly with time and location. The second type relates to the target: its size, shape and depth below the surface. The last group pertains to the measurement system: the receiver field of view and the laser beam divergence, both of which are controlled during experimentation. On the basis of the analytic considerations, the relative merits of the hybrid and lidar systems can be predicted.

1) For a wide field of view and a large, deep target, the magnitude of the radar target echo relative to that of the lidar should decrease.
2) With lidar, the clutter portion of the return signal, $H_i(f)$, increases as the beam footprint increases; however, with radar, the clutter should decrease.
3) The contrast, the ratio of the target return to clutter, should favor the hybrid scheme as the footprint-to-target size ratio increases and the field of view decreases.

To validate the benefits and understand the limitations of the hybrid detection scheme in the actual ocean environment, an ocean field test was designed and conducted. The following sections outline the specific goals of the ocean experiment and discuss the limitations of the field test. In addition, the hybrid lidar-radar system developed for ocean experimentation is described. Finally, results of the ocean experiment are presented and interpreted, and recommendations for future tests are discussed.

II. Design of the Hybrid Lidar-Radar Ocean Experiment

The primary objective of the experiment was to develop a hybrid lidar-radar system and to test this system in an ocean setting. This would provide insight into improvements which can be implemented in future systems and identify those parameters which affect the encoded microwave signal. To obtain this end result, three successive goals were defined for the ocean field test.

1) The first and most crucial objective was to design and assemble a hybrid lidar-radar system which could operate effectively in the ocean environment.
2) The second goal was to utilize the system to determine how well the integrity of the microwave subcarrier is preserved as it travels through water. This is a prerequisite to the introduction of more sophisticated detection and signal processing techniques to future hybrid lidar-radar systems.
3) The final aim was a) to evaluate experimentally how system variables affect the sensitivity of the hybrid system, and b) to compare the results with those predicted by analytical studies and laboratory experiments.

The next step involved selecting an appropriate test location. The site selected was a tower located approximately 1 mile from the shore of the Atlantic Undersea Test and Evaluation Center (AUTEC) on Andros Island, Bahamas. The advantages of this site include moderate cost, direct access to 10 m of clear ocean water, resemblance of a realistic lidar environment, and protection of experimental equipment. Since the tower was elevated only 12 m from the ocean surface, deploying underwater targets and aligning the system to detect these targets was relatively easy. The limitations of this site include invariant water quality, shallow-water depth, and a low-platform altitude. The low tower elevation resulted in a deviation of geometry from the aerial system. Specifically, the two orders of magnitude difference in altitude between the tower and an airborne platform required a larger beam divergence and receiver field of view to approximate the aerial situation. Other limitations include variables such as the random sea surface and the tilt of the flat underwater target. The effects of these various parameters on the results are discussed later.

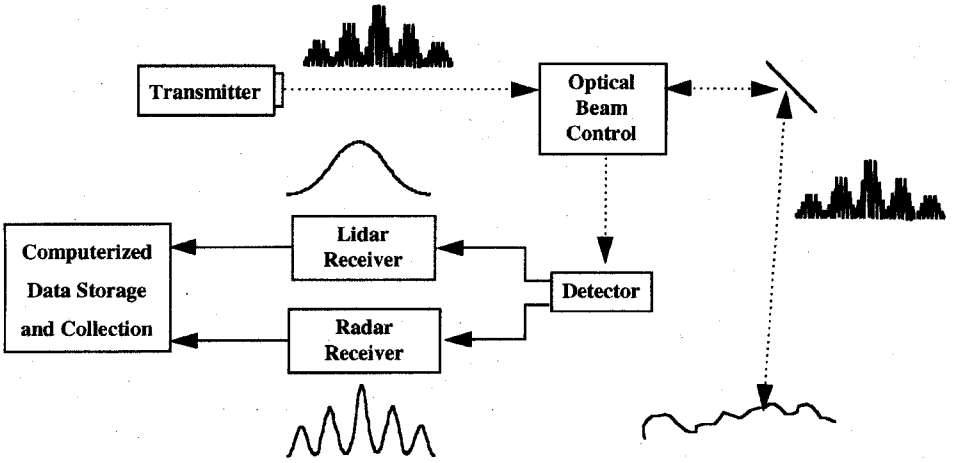

Fig. 2. Block diagram of the hybrid lidar-radar system for ocean experimentation. The microwave envelope is superimposed on the optical pulse. The lidar receiver recovers the pulse envelope, while the radar receiver filters the microwave envelope.

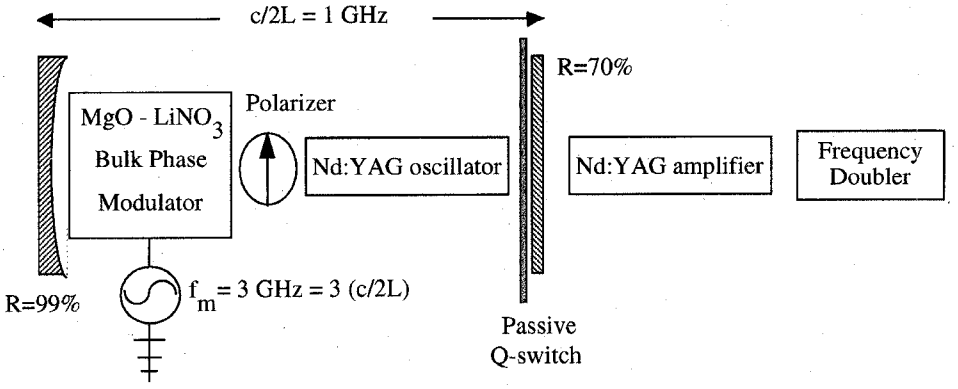

Fig. 3. Block diagram of the 3 GHz modulated, blue-green laser transmitter for the hybrid lidar-radar system. The passive Q-switch is an acetate sheet manufactured by Kodak. The input and output mirror reflectivities are 99% and 70%, respectively. The optical cavity is also resonant at the microwave frequency, which provides positive feedback for the modulation.

The principal task in attaining the experimental goals is developing a hybrid lidar-radar system for ocean experimentation. The challenge in constructing such a system lies in the dynamic range required to overcome the losses (>60 dB) incurred in the backscatter measurement. Furthermore, a method of modulating the high power optical transmitter at microwave frequencies must be found, and a high-speed, large-area optical detector to recover the microwave signal must be identified. The system that was designed and fabricated to meet these specifications is described in the following section.

III. Hybrid Lidar-Radar Experimental Setup

The full-scale hybrid lidar-radar system, shown in Fig. 2, contains four principal elements: the optical transmitter, the transceiver (optical beam control and detector), the lidar and radar receivers, and the signal processing apparatus. These subsystems are described next.

A. Modulated Transmitter

Various techniques were evaluated for producing a high-power (>1 kW), blue-green, microwave-modulated, stable optical pulse [3]. The configuration which met these specifications is shown in Fig. 3. This optical transmitter consists of a laser oscillator, an optical amplifier and a frequency doubler. The critical component is the oscillator, an optical cavity containing a flashlamp-pumped Nd:YAG rod, a 3-GHz phase modulator and a passive Q-switch. In this configuration, the microwave resonance of the optical cavity provided positive feedback for the modulation.

Six random samples of the modulated transmitter output are shown in Fig. 4. All the pulses exhibit one hundred percent modulation depth at 3 GHz and have good amplitude stability. The corresponding pulse frequency spectrums are shown in Fig. 5. Although the pulses contain some energy at the modulation frequency harmonics, the bulk of the signal energy is contained at 3 GHz. Other essential features of the modulated transmitter include a peak output power of 10 kW and good output beam quality. In addition, by appropriate choice of a low noise passive Q-switch, pulsewidths ranging from 6 to 20 nanoseconds were generated.

B. Transceiver

A detailed block diagram of the transceiver is shown in Fig. 6. Two optical lenses control the transmitter beam divergence, while a Fresnel lens focuses the return light onto the detector. An interference filter reduces the background light, and an iris inserted at the detector controls the receiver field of view. The optical detector is an intensified photodiode. This device contains an 8 mm GaAsP photocathode and a 1-mm GaAs p-i-n photodiode with a 10^3 low-noise gain [4]. The 3-

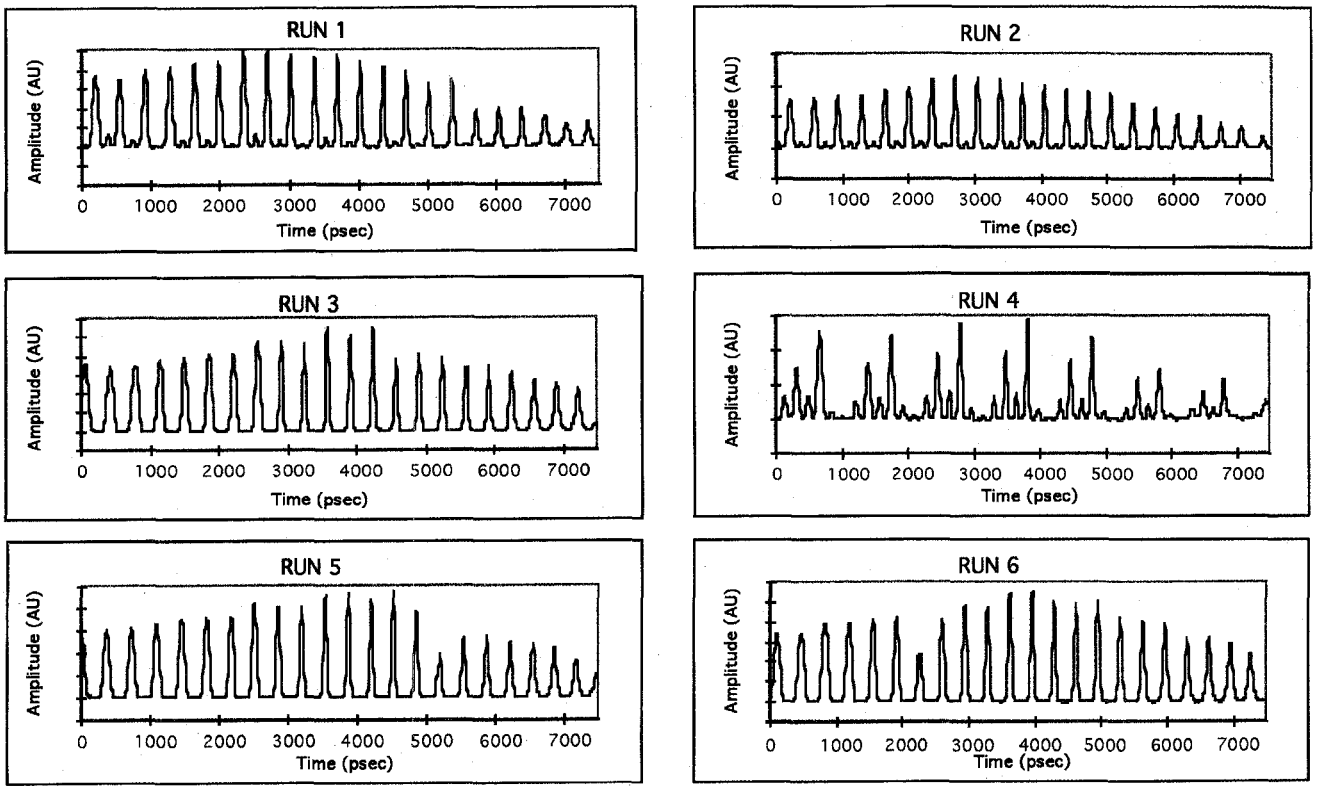

Fig. 4. Samples of the modulated transmitter output as detected by a high-speed streak camera. The pulses are 100% modulated at 3 GHz.

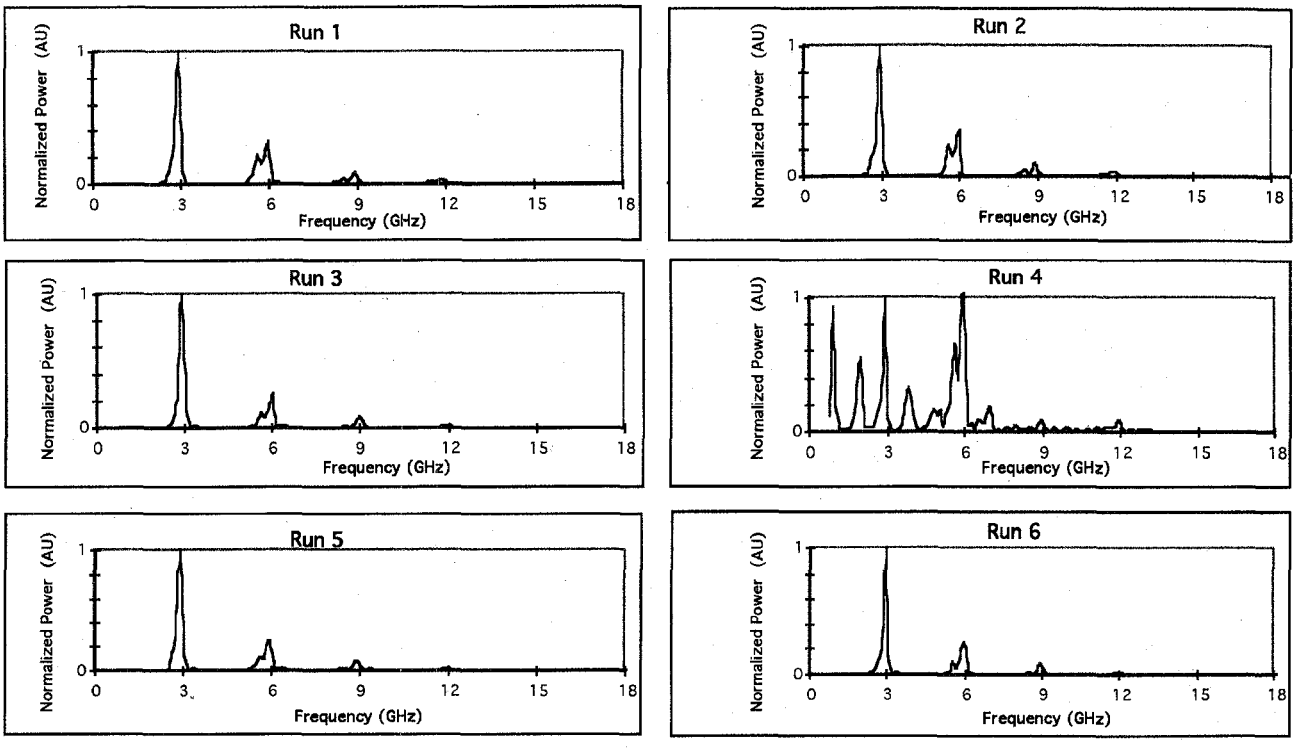

Fig. 5. Corresponding frequency spectra of the pulses shown in Fig. 3. The majority of signal energy is contained at 3 GHz.

dB bandwidth of the detector is 1 GHz, with a loss of nearly 20 dB at 3 GHz.

C. Radar and Lidar Receivers and Signal Processing

The output of the intensified photodiode is split into its high frequency (radar) and low frequency (lidar) components, which are processed independently. The radar receiver includes two low noise microwave amplifiers, a bandpass filter centered at 3 GHz, and a microwave detector. The lidar receiver contains a low-pass (100 MHz) filter. The radar and lidar signals are digitized and displayed simultaneously

TABLE I
RADAR-TO-LIDAR PEAK TARGET RETURN RATIOS (IN dB) FOR VARYING TARGET SIZE AND DEPTH AND RECEIVER FIELD OF VIEW. THE LARGEST DECREASE IN THE RATIO OCCURS WHEN THE TARGET SIZE IS INCREASED

Beam Divergence	-	Wide (40 millirad)	
Field of View	-	Narrow (10 millirad)	Wide (50 millirad)
Target Depth	Target size	dB	dB
3 m	0.15 m	-1.10	-1.15
	0.5 m	-7.96	-8.17
5 m	0.15 m	-1.18	-4.03
	0.5 m	-8.59	-9.75

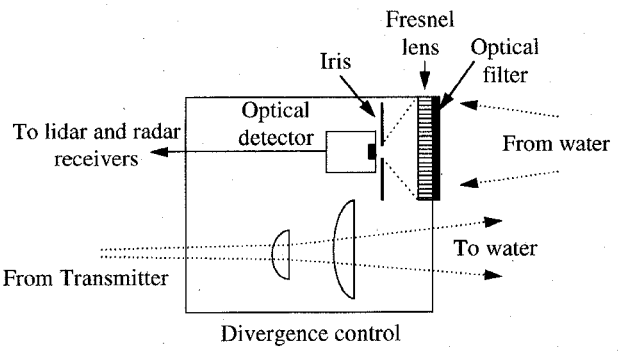

Fig. 6. Transceiver block diagram including the optical detector with associated optical focusing and filtering components and a mechanism to control the beam divergence and receiver field of view.

on two channels of a digitizing oscilloscope. An external computer controls the data collection and storage.

D. System Integration

The entire hybrid lidar-radar system was assembled and evaluated prior to the ocean test. The measured dynamic range is better than 90 dB. The transmitter beam divergence ranges from 1 to 40 milliradians (half-angle), while the receiver field of view is variable from 10 to 50 milliradians (half-angle). In the following section, the deployment of this system in the ocean experiment is discussed, and revisions to be included in future systems are considered.

IV. OCEAN EXPERIMENT TEST RESULTS

The success of the ocean experiment depended on the system performance and the microwave signal integrity. With these issues addressed, various tests could then be conducted to better understand the benefits and limitations of the new detection scheme. These subjects are discussed in the following paragraphs.

A. System Performance

The first experimental goal, as stated earlier, was to construct a hybrid lidar-radar system and to test it in the ocean environment. The entire system described above operated effectively and provided echoes with good signal-to-noise and stability.

B. Signal Quality

The preservation of the frequency and phase of the microwave envelope is critical to the performance of the hybrid lidar-radar system. All experimental observations confirm that the integrity of the microwave signal was retained. More specifically, several microwave interference effects indicated that the subcarrier phase information was maintained. Experimental and analytic studies identified four main sources of interference: the Fresnel lens in the receiver, the receiver field of view, the target size, and the sea surface fluctuation. Optical interference did not cause these effects since optical coherence is destroyed by scattering from the ocean surface and particulate matter. Conversely, path length differences on the order of microwave wavelength results in partial cancellation, and subsequent fading, of the microwave subcarrier. In the following paragraphs, the nature of the interference effects are discussed and experimental evidence of the microwave signal integrity is presented.

The compact, light-weight Fresnel lens, a standard element of lidar receivers, is a diffractive focusing device. This component creates a path length difference between the light which is incident on the lens edge and center. For the 15- cm Fresnel lens used in the receiver shown in Fig. 6, the path length difference produces a maximum phase difference of 113°, which decrease the radar return by 5 dB. This partial microwave cancellation was calibrated and incorporated in the data analysis. Replacing the Fresnel lens with a conventional refractive lens will eliminate this interference problem in future systems.

The second source of interference arises from the receiver field of view. Wide receiver fields of view subtend light at large angles which also produces microwave subcarrier fading. In the experiments, the receiver field of view was varied from 10 to 50 milliradians, and the radar-to-lidar target return ratio at each depth was measured. The results are summarized in Table I. For a wide beam divergence (40 milliradians) and narrow field of view, the radar-to-lidar target return ratios for each target diameter decreased by less than 1 dB as the depth was varied from 3 to 4.6 m. However, as the field of view and target depth increased, the radar-to-lidar target ratio decreased by approximately 3 dB for the small target and by half this value for the large target. This implies that the signal included in the wide field of view and deep depth measurement included scattered light which slightly decreased the microwave return, as expected. In an airborne platform, the higher altitude requires a smaller field of view for the same surface viewing area; therefore, the microwave subcarrier fading should decrease.

The third interference effect was caused by the target size. The path length difference, Δl, due to a flat target with

TABLE II
STATISTICS (STANDARD DEVIATION/AVERAGE) OF THE LIDAR AND RADAR TARGET RETURNS FOR VARYING TARGET SIZE AND DEPTH AND RECEIVER FIELD OF VIEW

Beam Divergence	-	wide (40 mR)			
Field of View	-	narrow (10 mR)		wide (50 mR)	
Target Depth	Target size	lidar	radar	lidar	radar
3 m	0.3 m	0.28	0.68	0.25	0.26
	1 m	0.30	0.33	0.27	0.21
4.6 m	0.3 m	0.32	0.58	0.41	0.43
	1 m	0.31	0.44	0.26	0.35

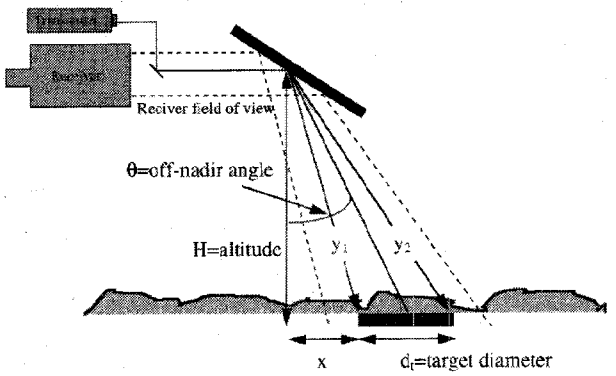

Fig. 7. Diagram of the tower experiment geometry resulting in path length differences from the target diameter, d_t, off-nadir angle, θ, and platform elevation, H.

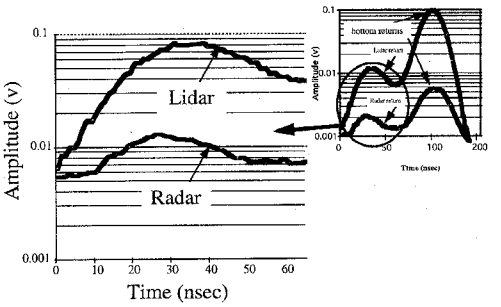

Fig. 8. Lidar and radar backscatter waveforms obtained with a narrow beam divergence and a wide field of view. The insert identifies the portion of the return signals which are displayed in the figure. The radar backscatter signal is suppressed by 9 dB relative to the lidar backscatter return.

diameter d_t (see Fig. 7) can be calculated as follows:

$$\Delta l = y_2 - y_1$$

where

$$y_1 = \sqrt{x^2 + H^2}, \quad y_2 = \sqrt{(x + d_t)^2 + H^2}$$
$$x = H\tan(\theta) - \frac{d_t}{2}.$$

The corresponding microwave phase shift, $\Delta\phi_{mw}$, is

$$\Delta\phi_{mw} = \frac{\Delta l}{\lambda_{mw}} \times 360^\circ$$

where λ_{mw} is the microwave wavelength and the remaining variables are defined in Fig. 7. Thus, as the target diameter and off-nadir angle (or the target tilt angle relative to the receiver plane) increase, the microwave subcarrier fading increases. To verify this, the size of the flat underwater target was varied from 0.3 to 1 m with a constant off-nadir angle. As shown in Table I, the radar-to-lidar target return ratio decreased (approximately 7 dB) as the target diameter increased. Thus, the experimental data confirm that the integrity of the microwave signal is preserved, and the dominant origin of microwave subcarrier fading was the large, flat underwater target. The effect of the target size on the hybrid system performance will be addressed in future experiments.

The last source of microwave subcarrier fading was the scattering of the optical beam from the fluctuating sea surface. Small, randomly distributed capillary waves on the sea surface tend to break the impinging radiation into multiple beams [5]. Since each beam has a different path length from the sea surface to the target and back to the receiver, destructive interference may occur, thereby adversely affecting the performance of the hybrid scheme. To study this random phenomenon, the statistics of the radar and lidar target returns were examined. Specifically, the variance of multiple shots was evaluated with the target size and depth and field of view as variables (see Table II). If these capillaries have a significant effect on the hybrid system, the variance of the radar target return is expected to be greater than that of the lidar return.

Inspection of the data summarized in Table II shows that the variances for the radar and lidar target returns remain relatively equal. The only significant increase in variance for the radar signals occurs for a narrow field of view and small target size. This result, however, is attributed to the fact that for this particular set of parameters, the lidar return is dominated by the water backscatter signal, which is independent of surface effects. Therefore one can conclude that the capillaries do not significantly decrease the effectiveness of the hybrid system.

Although these interference effects increased the complexity of the experimentation and subsequent data analysis, their existence indicated that the microwave signal integrity was maintained throughout the range of measurements. Since the integrity of the propagating microwave subcarrier is preserved, a set of experiments was performed to evaluate the sensitivity of hybrid lidar-radar relative to lidar as a function of various system and environmental variables.

C. Clutter Reduction and Contrast Enhancement

Prior theoretical and laboratory studies predicted that the hybrid detection scheme suppresses the backscatter clutter and therefore enhances the contrast of small, shallow underwater targets. To test this premise, the lidar and radar backscatter

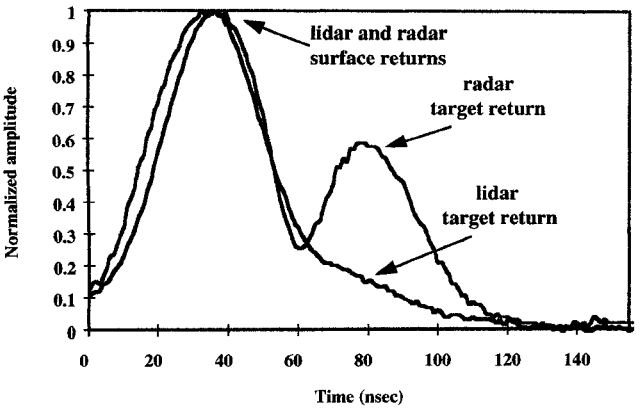

Fig. 9. Lidar and radar target returns obtained with the following set of parameters: wide-beam divergence, narrow field of view, 0.3-m target at 4.6-m depth. The radar target contrast is improved relative to the lidar return due to the backscatter reduction produced by the hybrid detection scheme.

signal levels were measured simultaneously. The optical pulse was transmitted at a slight angle to the water surface to minimize surface reflections. A representative sample of the measured return signal is displayed in Fig. 8. Since the surface return is absent, the steadily rising segment of the backscatter signal represents the pulse as it enters the water. The peak occurs when the entire pulse has entered the water. The signal subsequently decays exponentially due to absorption and scattering of the optical beam by the water column. For the narrow beam divergence (<0.1 m spot size) experiment, the radar backscatter signal level is decreased by 9 dB relative to the lidar backscatter magnitude. The difference in the backscatter amplitudes is expected to expand as the beam footprint increases to that which is typical in an aerial lidar system (approximately 10 m).

The backscatter reduction of the hybrid detection scheme is accompanied by a corresponding enhancement of the underwater target contrast. The best results are expected when the lidar return is contrast limited. This scenario occurs when the target is small compared to the lidar footprint and is located at a relatively shallow depth. Furthermore, the narrow field of view minimizes the microwave subcarrier fading. Thus, the variation of the footprint-to-target size ratio and receiver field of view should have a marked influence on the performance of the hybrid system.

Two different footprint-to-target size ratios were obtained by using a large beam divergence (1-m spot diameter) in combination with two different target sizes (0.3 and 1 m diameters). In addition, with each scenario, the receiver field of view was varied from narrow (10 milliradians) to wide (50 milliradians) to determine its effect on the target contrast. Although the target contrast is obtained by measuring the target return-to-background ratio, the shallow water depth at the test site prohibited the quantification of this information. However, results indicated that the hybrid system produced an improvement in target contrast when the 0.3 m target was detected with a wide beam divergence and a narrow field of view, as predicted by earlier studies. A sample of the lidar and radar returns obtained with this set of parameters is shown in Fig. 9. This figure clearly demonstrates that the contrast of the radar target return is improved as compared to the corresponding lidar return. This result is a direct consequence of the backscatter clutter reduction produced by the hybrid detection scheme.

V. Conclusion and Future Work

The design and realization of an ocean experiment utilizing a novel hybrid lidar-radar detection scheme has been reported. The conclusions of the ocean experimentation and subsequent data analysis are as follows.

1) A hybrid lidar-radar system can be built which performs well in the ocean environment. Specifically, a high-power, microwave-modulated, blue-green optical pulse was generated and detected.
2) The microwave subcarrier integrity is preserved due to the observance of microwave interference effects. Therefore, more sophisticated detection and signal processing schemes can be implemented in future systems.
3) Use of the hybrid detection scheme results in a reduction of backscatter clutter and an improvement in underwater target contrast relative to conventional lidar. Therefore, it is desirable to continue to explore this technique for underwater target detection.

The results obtained in this first-of-a-kind experiment encourage additional tests incorporating more sophisticated radar modulation and detection schemes. These experiments will determine the optimal modulation and detection technique for specific target size and depth scenarios. In addition, future system improvements and experiments were identified by fielding the hybrid lidar-radar system in the ocean environment. The next generation of hybrid lidar-radar systems will include a better receiver (improved optical detector and refractive optics). Proposed tests include experiments with different modulation frequencies, water types and depths, and platform altitudes.

Acknowledgment

The authors would like to thank the AUTEC staff, especially C. Harvey, D. Hutchison, and G. Cantelo, for their help and guidance during the field test. The authors would also like to acknowledge Dr. S. Ackleson for his support through the Office of Naval Research 6.2 funding.

References

[1] L. Mullen, A. Vieira, P. R. Herczfeld, and V. M. Contarino, "Application of RADAR technology to aerial LIDAR systems for enhancement of shallow underwater target detection," *IEEE Trans. Microwave Theory Tech.*, vol. 43, pp. 2370–2377, Sept., 1995.

[2] L. Mullen, P. R. Herczfeld, and V. M. Contarino, "Analytical and experimental evaluation of an optical fiber ocean mass simulator," *IEEE Microwave Guided Wave Lett.*, vol. 4, pp. 17–19, Jan, 1994.

[3] L. Mullen, A. Vieira, P. R. Herczfeld, and V. M. Contarino, "Microwave-modulated transmitter design for hybrid LIDAR-RADAR," in *Proc. 1995 IEEE MTT-S Int. Microwave Symp.*, May 1995, pp. 1495–1498.

[4] R. La Rue, J. Edgecumbe, G. Davis, S. Gospe, and V. Aebi, "High quantum efficiency photomultiplier with fast time response," *SPIE Photodetectors and Powermeters*, vol. 2022, pp. 64–73, July 1993.

[5] W. C. Brown and A. K. Majumdar, "Point-spread function associated with underwater imaging through a wavy air-water interface: theory and laboratory tank experiment," *Appl. Opt.*, vol. 31, no. 36, pp. 7650–7659, Dec. 1992.

Linda J. Mullen received the B.S. degree in electrical engineering from Trenton State College, Trenton, NJ, in 1992, the M.S. degree in electrical engineering from Drexel University, Philadelphia, PA, in 1993, and the Ph.D. degree in electrical engineering from Drexel University.

Her thesis focused on the application of microwave technology to optical modulation and detection in underwater laser-radar system design.

Dr. Mullen received the 24th European Microwave Prize in 1994 for her thesis work.

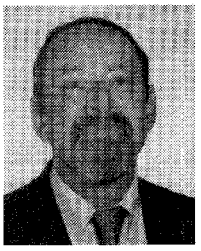

Peter R. Herczfeld (S'66–M'67–SM'89–F'91) born in Budapest, Hungary, in 1936. He received the B.S. degree in physics from Colorado State University in 1961, the M.S. degree in physics in 1963, and the Ph.D. degree in electrical engineering in 1967, both from the University of Minnesota, St. Paul.

Since 1967, he has been on the faculty of Drexel University, Philadelphia, PA, where he is a Professor of Electrical and Computer Engineering. He has published over 300 papers in solid-state electronics, microwaves, photonics, solar energy, and biomedical engineering. He is the Director of the Center for Microwave-Lightwave Engineering at Drexel, a Center of Excellence that conducts research in microwaves and photonics. He has served as project director for more than seventy projects.

A member of APS, SPIE, and the ISEC, Dr. Herczfeld is a recipient of several research and publication awards, including the Microwave Prize in 1986 and 1994.

Vincent M. Contarino received the B.S. degree in physics from Lafayette College, Easton, PA, in 1975, the M.S. degree in engineering and computer science from Pennsylvania State University, University Park, in 1981, and the Ph.D. degree in electrical engineering from Drexel University, Philadelphia, PA, in 1991.

He has been with NAWC (Warminster) since 1977. His background has been in the development of pulsed blue-green air-to-underwater laser-radar systems with research in microwave interactions, microwave optical modulation, and lidar component development.

Dr. Contarino received the 16th European Microwave Prize in 1986 for his doctorate work at Drexel University and was a corecipient of the 24th European Microwave Prize in 1994.